ADVANCED MATERIALS INTERFACES
www.advmatinterfaces.de

Biofunctionalization of Graphene-Based FET Sensors through Heterobifunctional Nanoscaffolds: Technology Validation toward Rapid COVID-19 Diagnostics and Monitoring

Esteban Piccinini, Gonzalo E. Fenoy, Agustín L. Cantillo, Juan A. Allegretto, Juliana Scotto, José M. Piccinini, Waldemar A. Marmisollé, and Omar Azzaroni**

The biofunctionalization of graphene field-effect transistors (GFETs) through vinylsulfonated-polyethyleneimine nanoscaffold is presented for enhanced biosensing of severe acute respiratory-related coronavirus 2 (SARS-CoV-2) spike protein and human ferritin, two targets of great importance for the rapid diagnostic and monitoring of individuals with COVID-19. The heterobifunctional nanoscaffold enables covalent immobilization of binding proteins and antifouling polymers while the whole architecture is attached to graphene by multivalent π–π interactions. First, to optimize the sensing platform, concanavalin A is employed for glycoprotein detection. Then, monoclonal antibodies specific against SARS-CoV-2 spike protein and human ferritin are anchored, yielding biosensors with limit of detections of 0.74 and 0.23 nM, and apparent affinity constants (K_D^{GFET}) of 6.7 and 8.8 nM, respectively. Both biosensing platforms show good specificity, fast time response, and wide dynamic range (0.1–100 nM). Moreover, SARS-CoV-2 spike protein is also detected in spiked nasopharyngeal swab samples. To rigorously validate this biosensing technology, the GFET response is matched with surface plasmon resonance measurements, exhibiting linear correlations (from 2 to 100 ng cm^{-2}) and good agreement in terms of K_D values. Finally, the performance of the biosensors fabricated through the nanoscaffold strategy is compared with those obtained through the widely employed monopyrene approach, showing enhanced sensitivity.

1. Introduction

The coronavirus disease 2019 (COVID-19) pandemic has profoundly changed society's need for diagnostic tools.[1] This is due to the fast transmission rate of severe acute respiratory-related coronavirus 2 (SARS-CoV-2) and the fact that some of the patients are asymptomatic but still capable of transmitting the virus, serving as hidden drivers of the pandemic. Moreover, the features of the virus and the disease seem to trigger superspreading events provoking massive infection.[2,3] In this regard, diagnostics play a crucial role in making timely decisions on the isolation of infected people for slowing or stopping the spread of COVID-19 disease. World Health Organization has formulated a guideline, named ASSURED (Affordable, Sensitive, Specific, User-friendly, Rapid and robust, Equipment-free and Deliverable to end-users) as a benchmark to identify the most suitable diagnostic tools for such situations.[4] Although antibody (Ab)-based serological test meets most of these features, its relevance for COVID-19 diagnostic purposes is limited because the generation of Abs against SARS-CoV-2 in the body takes a substantial amount of days after infection.[5,6] To rapidly detect and isolate infected people during the first days of their diseases, spike or nucleocapsid antigen tests can be used.[5,7] On the other hand, some test methods and diagnostic products present sensitivities lower than needed to stop COVID-19 spreading.[4] For instance, it was reported the sensitivity of COVID-19 Ag Respi-Strip (Coris Bioconcept, Belgium) and NADAL COVID-19 Ag Test (Nal Von Minden GmbH, Germany), both antigen test products for nasopharyngeal swab samples, ranges from 30% to 50%.[8,9] To overcome this issue, tests based on ultrasensitive techniques are being developed to reach sensitivities similar to reverse-transcription polymerase chain reaction (RT-PCR), the gold standard COVID-19 diagnostic method.

E. Piccinini, G. E. Fenoy, A. L. Cantillo, J. A. Allegretto, J. Scotto, W. A. Marmisollé, O. Azzaroni
Instituto de Investigaciones Fisicoquímicas Teóricas y Aplicadas (INIFTA)
Departamento de Química, Facultad de Ciencias Exactas
Universidad Nacional de La Plata (UNLP)
CONICET. 64 and 113, Buenos Aires 1900, Argentina
E-mail: este.piccinini@gmail.com; azzaroni@inifta.unlp.edu.ar
A. L. Cantillo, J. M. Piccinini
GISENS BIOTECH
Buenos Aires C1414BPV, Argentina

The ORCID identification number(s) for the author(s) of this article can be found under https://doi.org/10.1002/admi.202102526.

DOI: 10.1002/admi.202102526

Among the currently available antigen rapid detection methods, the biosensing through nanomaterial-based field-effect transistor (FET) has several advantages, including high sensitivity and virtually instantaneous measurements using small sample volume.[10–12] Moreover, FET electronic measurements can be easily digitalized for a quicker tracking of exposed individuals and coordinating case assignments with health care facilities.[13] These features make nanomaterial-based FETs ideal transducers for RE-ASSURED tests, an acronym for real-time connectivity and ease of specimen collection (RE) combined with ASSURED.[14] In particular, graphene field-effect transistors (GFETs) are one of the most attractive systems for biosensing,[15,16] since graphene, a 2D sheet of carbon atoms with high conductivity and good chemical stability, secures high signal-to-noise ratio and great detection sensitivity.[17,18]

Although the GFET technology is suitable for immunological rapid tests, the launch of such commercial product is still presenting some challenges: 1) Most of reported GFET devices have complex designs which are useful for research activities in a laboratory but are hardily adaptable to user-friendly and portable tests.[10,19] 2) They are usually prepared by protocols that are incompatible with wafer-scale mass production. For instance, although chemical vapor deposition (CVD) of graphene from a carbon feedstock gas at high temperatures on Cu surfaces is the commonly chosen method given its cost-quality ratio, it requires some steps such as Cu etching and graphene transfer that are not completely adapted for large-scale production.[20–22] As an appealing alternative, GFET sensors prepared from reduced graphene oxide (rGO) endow good semiconducting properties and high performance for biosensing applications.[23–25] Moreover, this method could be easily realized in microchip foundries. 3) Finally, there is a need for a binding approach suitable to attach recognition elements to graphene surfaces with enhanced stability. In this regard, the covalent modification of graphene induces lattice defects that hinder charge transport and reduce the FET transconductance.[26–28] On the other hand, traditional strategies, such as monopyrene docking on graphene by π–π interactions, are susceptible to desorption, particularly if highly charged or hydrophilic molecules are bonded.[29–32] In this regard, we have recently described the construction of vinylsulfonated-polyethyleneimine (VS-PEI) nanoscaffolds for performing the immobilization of both recognition and antifouling elements on graphene.[33] By employing this strategy, binding proteins and amino-terminated polyethyleneglycol (PEG) can be covalently bound to VS-PEI, while the whole architecture is attached to graphene by multivalent π–π interactions. Interestingly, the whole bio-interface was demonstrated to be more stable and presented better antifouling properties in comparison with that the obtained by a monopyrene-based approach. Moreover, this approach did not disrupt the aromatic chemical structure of graphene, maintaining its semiconducting properties. Although there are some reports of sensing platforms prepared with Abs adsorbed onto PEI-modified graphenic surfaces[34–37] the VS-PEI nanoscaffold approach has the advantages of presenting covalent-like stability, even in strong surfactant solutions, making possible the sensor regeneration for reusing, and the capacity of anchoring both Abs and antifouling elements.[33]

Compared with conventional SARS-CoV-2 antigen immunoassays, for example, ELISA and lateral-flow tests,[7,38] GFET sensing devices modified the heterofunctional VS-PA scaffolds displaying recognition and antifouling elements could have the following advantages: 1) simple digitization of the output data that could be used to improve medical record systems, that is, rapid access to information concerning a patient's health care; 2) GFET technology is fully compatible with the development of standalone smartphone-based biosensors; 3) only one type of recognition element (e.g., a capture Ab) is needed, whereas antigen immunoassay tests require the use of capture Abs, detector Abs, and nanoparticles or enzymes for the readout; 4) GFET test methodology is simpler and faster than ELISA since it does not require washing steps, incubation in solution with enzyme linked to detector Ab, enzymatic reaction, and a subsequent readout step with an additional laboratory equipment; 5) the activity of the Ab bound to VS–PEI on graphene could be restored with regeneration solutions,[33] a feature that is not accessible with lateral-flow tests, but may be particularly beneficial for reusing at-home antigen tests.

In this work, we report the design and construction of GFET biosensors for the fast and reliable detection of SARS-CoV-2 spike protein and human ferritin, both targets of major importance for a rapid diagnostic and monitoring of COVID-19. The biosensors were prepared from GFETs manufactured in commercial fabrication facilities. A complete electrochemical characterization of the GFET devices was carried out to assess the reproducibility, transistor sensitivity (in terms of transconductance, g_m), signal-to-noise ratio, and long-term stability in buffer medium. Then, through a straightforward surface engineering of graphene, VS-PEI nanoscaffolds were constructed on GFETs to covalently bind recognition and antifouling elements. To optimize this approach, a well-known lectin (as binding protein) with a high affinity against glycoproteins (as targets) was used as a model system. Real-time glycoprotein detection was studied in buffers of high and low ionic strength. Then, the optimized protocols were used to anchor monoclonal antibodies (mAbs) specific against SARS-CoV-2 spike protein and human ferritin for the detection of both targets. Sensing features such as dynamic range, limit of detection (LOD), specificity, and apparent K_D were obtained. Furthermore, target adsorbed mass was studied by surface plasmon resonance (SPR) spectroscopy. We show and discuss the correlation between the GFET response and the adsorbed surface mass, and compare the K_D obtained from both techniques. Finally, we show the outperformance of GFETs biosensors prepared by the VS-PEI nanoscaffolds approach with respect to those obtained with a commonly used monopyrene approach.

2. Results and Discussion

2.1. Electrical Characterization and Functionalization of the GFETs

For the implementation of graphene FETs as a suitable technology to be used in biosensing products, the demonstration of scalability, high sensitivity, and good device-to-device reproducibility is critical. Toward this aim, certain figures of merit

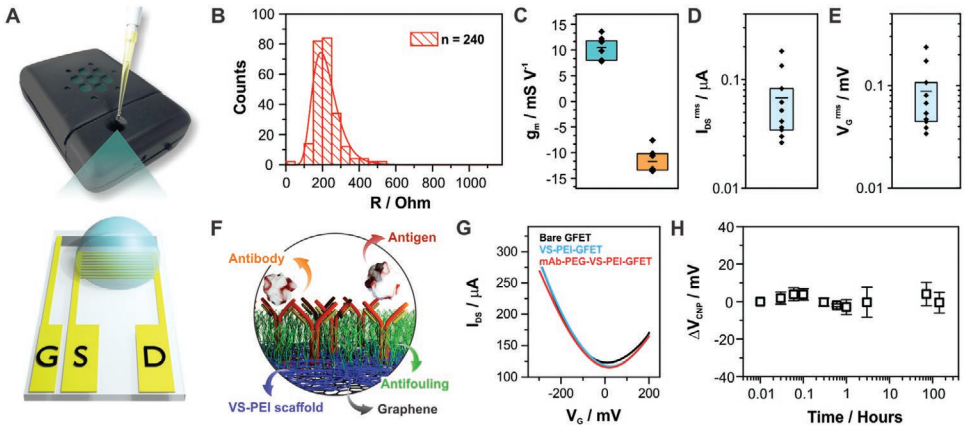

Figure 1. A) Photograph of the portable and wireless field-effect measurement station and scheme of a GFET sensor. B) Histogram of electrical resistance for 240 GFETs prepared with a wafer-scale method and randomly selected from independent production batches. Different sensing features were obtained from electrolyte-gated GFET measurements for nine randomly selected sensors: C) transconductance (g_m) normalized by V_{DS} = 0.05 V for the hole (orange) and electron (turquoise) branches; D) integrated I_{DS} current noise (I_{DS}^{rms}); and E) gate-source potential noise (V_{GS}^{rms}). Data are presented with a boxplot (values within 25th and 75th percentile) and the average value is represented with a solid line. F) Scheme of the VS-PEI nanoscaffold on a GFET sensor. G) Transfer characteristic curve for a bare GFET (solid line) and the same sensor after its surface modification with VS-PEI (blue line), and subsequently with both mAb-spike protein and PEG (red line). H) ΔV_{CNP} as a function of time for three GFETs modified with the mAb specific to SARS-CoV-2 spike protein. Electrolyte-gated measurements were performed with PBS buffer pH 7.4 and V_{DS} = 0.05 V.

of the transistors were evaluated. Electrical measurements were performed employing a portable FET measurement station and ready-to-sense GFETs (**Figure 1**A and Figure S1, Supporting Information). In Figure 1B the electrical resistance measured for 240 transistors produced with rGO and using a previously reported wafer-scale method[39] is shown. The resistance mean value was 222 Ω with a standard deviation (SD) of 71 Ω, and the histogram satisfactorily fits with a lognormal distribution (see Figure S2A, Supporting Information, for probability P-P plot). In the group of 240 chips, only 5 presented an out of range (too low or too high) resistance to be used for sensing field-effect. Therefore, the unsuccessful rate in the device fabrication was 2%, 15-fold better than GFETs prepared by other upscaled methods.[40] Then, 9 chips were randomly selected from different batches to assess the field-effect properties and sensing features in Phosphate buffer saline (PBS) buffer (Figure S2B,C, Supporting Information). Transconductance (g_m) normalized by V_{DS} was calculated from transfer characteristics curves for the hole and electron branches (Figure 1C). Average values of 10.5 and –11.7 mS V^{-1} were obtained, respectively. These values are many times higher with respect to silicon nanowire FETs,[41] organic FETs,[42,43] and other graphene-based FETs.[19,40,44,45] The higher the transconductance, the greater the sensing amplification of the FET when the sensing strategy is based on monitoring changes in I_{DS} at a constant V_G. It is also possible to observe a high homogeneity in terms of g_m, since all the devices displayed a g_m above 0.7 times the average value; a criterion previously considered as a good GFET reproducibility.[44] The minimum in I_{DS} occurs at a particular gate voltage, referred to as the charge neutrality point (V_{CNP}). This point corresponds to the conditions for which the Fermi energy in the graphene channel is, on average, closest to the energy with a minimum density of states. V_{CNP} is a relevant parameter to be monitored for different biosensing applications.[16,24,46] For the same group of devices, the V_{CNP} change (ΔV_{CNP}) in PBS solution was obtained (Figure S2D, Supporting Information) with a mean value of –3 mV. Moreover, V_{GS}^{rms} is an important parameter to evaluate the real noise of the sensors, which is defined as the ratio between the integrated I_{DS} current noise (I_{DS}^{rms}) of the transistor and its transconductance.[47] Figure 1D,E shows I_{DS}^{rms} and V_{GS}^{rms} of the devices, with mean values of 0.068 µA and 0.088 mV, respectively.

For the robust immobilization of affinity-proteins and antifouling polymers, surface engineering of GFETs through heterobifunctional supramolecular-covalent scaffolds based on VS-PEI (Figure 1F) was conducted as previously described.[33] Briefly, VS-PEI scaffolds were constructed onto GFETs by three simple surface modification steps: 1) the adsorption of pyrenebutanoic acid succinimidyl ester (PBSE) on graphene; 2) the fast reaction of polyethyleneimine (PEI) in aqueous solutions with surface-bound PBSE; and 3) the modification of remaining primary amine groups with divinylsulfone (DVS, a well-known cross-linker of −SH, $-NH_2$, and −OH groups via Michael type addition),[48–51] yielding VS-PEI on graphene. In these scaffolds, one side binds graphene through multivalent π–π interactions with pyrene groups, and the other side presents vinylsulfonated pending groups that can be used for covalent binding. As previously reported,[33] the preparation of VS-PEI was characterized by Raman spectroscopy; the step-by-step construction of the nanoscaffold on rGO and the subsequent covalent immobilization of the binding-protein and the antifouling elements was corroborated by spectroscopic ellipsometry, SPR spectroscopy, and contact angle goniometry. A summary of the characterization is described in Tables S1 and S2, Supporting Information.

Transfer characteristic curves were recorded before and after the modification steps (black and blue lines in Figure 1G). The calculated g_m values are shown in Figure S3A, Supporting Information, while the V_{CNP} values for the curves are exhibited in Figure S3B, Supporting Information. A shift in the V_{CNP} to more positive values is observed after the modification with the VS-PEI nanoscaffold, probably ascribed to the n-type doping occurring upon the modification of the transistors with

the pyrene-like molecule, the polyelectrolyte, and the reaction with DVS.[52] Moreover, the incorporation of the rest of the elements of the assembly (PEG and mAb) yields a diminution in this shift, although the V_{CNP} value does not reach that of the bare device. This result can be ascribed to a diminution of the doping caused by the VS-PEI scaffolds, since some of these moieties are employed in order to anchor the recognition entities. From these results it can be concluded that our functionalization approach does not disrupt the semiconducting properties of graphene, as previously demonstrated.[33]

Next, recognition elements were bound to VS-PEI scaffolds prepared onto the graphene transistor. Three affinity-proteins were used as recognition elements: 1) Concanavalin A (ConA), a well-known lectin with high affinity to glycans; 2 a mAb specific to SARS-CoV-2 spike protein; 3) a mAb specific to human ferritin. After that, the sensors were modified with PEG, for avoiding nonspecific adsorption, followed by blocking the remaining vinylsulfonated-groups with ethanolamine (ETA). It should be noted that throughout this modification approach, GFETs retain the sensitivity after anchoring both the recognition and the antifouling elements (see transfer characteristic curves in Figure 1G, red line, and their transconductances in Figure S3, Supporting Information).

On the other hand, the stability of the GFETs modified with the mAb specific to SARS-CoV-2 spike protein was studied in PBS to ensure the reliability of the recording system. Transfer characteristics curves were recorded during 100 h; then ΔV_{CNP} referred to the initial CNP was calculated (Figure 1H). Minor ΔV_{CNP} differences were obtained during the whole study, evidencing high stability of the GFETs electronic properties which is of paramount importance to maintain a good sensitivity. Therefore, the coplanar microelectronic design of these devices with an Ag/AgCl gate overcomes the low V_{CNP} stability previously observed for GFETs made with Au gates.[44]

2.2. Detection of Glycoprotein-Lectin Recognition

First, as a model system for the evaluation of the GFET technology for the detection of proteins through biological affinity, we explored the recognition of the glycoprotein glucose oxidase (GOx) by the ConA lectin. ConA exists as a tetramer at neutral pH, and each monomer contains one carbohydrate-binding site, specific to α-D-mannose and α-D-glucose.[53] On the other hand, GOx presents α-D-mannose residues enabling a high-affinity recognition to ConA.[54,55] We take advantage of this well-known system to study the field-effect response after GOx binding to ConA immobilized on GFETs (**Figure 2**A). To this end, the lectin was covalently attached to graphene by the VS-PEI scaffold, followed by PEGylation and blocking with ETA.

Figure 2B shows the response of a ConA-modified GFET while increasing the concentration of GOx employing a buffer HEPES solution of low (0.1×) ionic strength, while Figure 2C shows the obtained results for both low and high ionic strength conditions. From Figure 2B, the addition of GOx solutions causes a change in the I_{DS}, ascribed to the biorecognition of GOx by ConA. The recognition-mediated assembly of GOx is observed as a decrease in I_{DS}, coherent with negatively charged species adsorption, that is, n-doping effect since GOx has negative charges at the pH employed (the isoelectric point of GOx is 4.2[56]). Moreover, from Figure 2C, the devices show a higher response (i.e., a higher change in I_{DS}) while performing the measurements in low ionic strength solution. For this solution, the amplitude of the biosensor response is 201 ± 32% higher than the measurements performed in high ionic strength solution. This effect has already been reported in FETs and it is ascribed to more noticeable changes in graphene doping due to a diminution of the ionic screening (i.e., an increase of the Debye length) with the decrease of the ionic strength.[18,19,57] In order to obtain the apparent affinity constant from the GFET

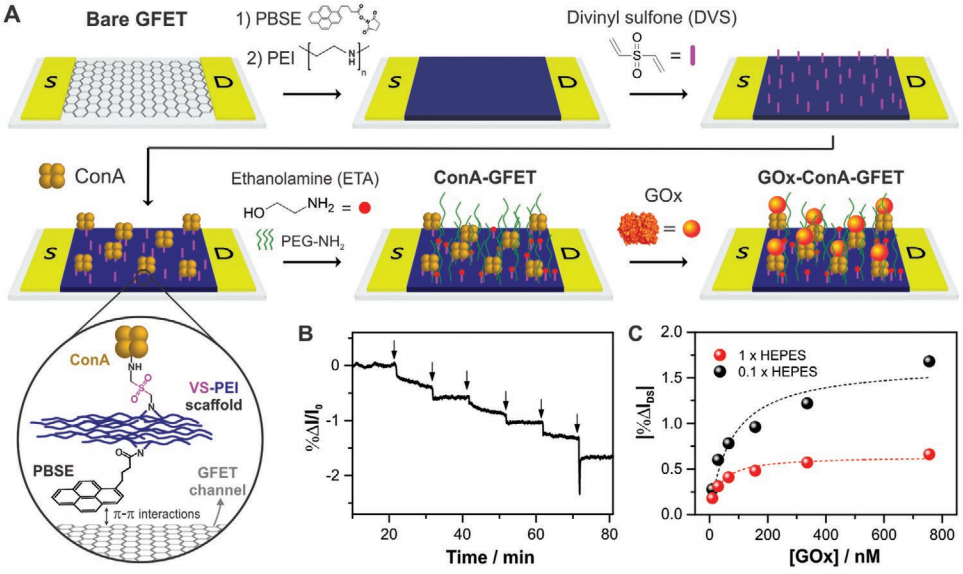

Figure 2. A) Scheme of the biosensors functionalization process employing the VS-PEI strategy. B) Relative change in I_{DS} for a ConA-GFET upon the addition of different GOx concentrations (V_{DS} = 50 mV, V_{GS} = −250 mV, HEPES buffer pH 7.4 with 0.5 mM $CaCl_2$). C) Results obtained at different ionic strengths and Hill (n = 1) fitting.

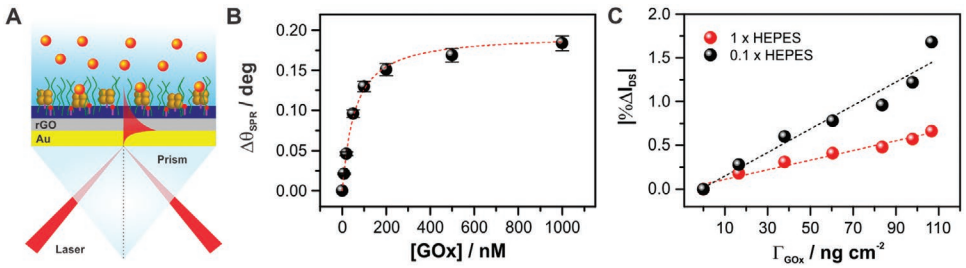

Figure 3. A) Scheme of the SPR measurement setup. B) Change in the surface plasmon resonance minimum reflectivity angle shift ($\Delta\theta_{SPR}$) upon increasing GOx concentration. C) Correlation between I_{DS} response and GOx surface mass density obtained from GFET and SPR measurements, respectively. Both measurements were carried out in HEPES buffer pH 7.4 with 0.5 mM $CaCl_2$.

measures (K_D^{GFET}), the relative changes in I_{DS} current were fitted to a noncooperative Hill model. The obtained K_D^{GFET} values were 33 ± 7 nM (R^2 = 0.95) and 75 ± 28 nM (R^2 = 0.90) for measurements in high and low ionic strength, respectively. Our values are in close agreement with previous works.[58]

With the aim of validating the GFET-based detection method and evaluating the response of the devices in terms of the GOx adsorbed mass, SPR measurements were performed employing the same interfacial architecture on graphene-modified SPR sensors to determine the amount of immobilized protein. **Figure 3**A shows a scheme of the measurement setup and the interfacial architecture constructed on the SPR sensors. Next, GOx adsorption on this platform was evaluated, and results are shown in Figure 3B. The SPR minimum reflectivity angle shift ($\Delta\theta_{SPR}$) was fitted to a noncooperative Hill model, yielding a K_D^{SPR} of 59 nM (R^2 = 0.99), in excellent concordance with GFETs results. Moreover, Figure 3C shows the relative changes in I_{DS} versus GOx surface mass density obtained from GFET and SPR measurements, respectively. A higher sensitivity of the devices in lower ionic strength electrolyte solution is evidenced because of a larger Debye screening length. Interestingly, it can be observed that the dependence of the biosensor electronic response with the GOx surface coverage is linear, thus validating the use of our GFET devices modified with binding proteins, through the VS-PEI scaffold strategy, for the detection of charged protein targets. These features together with the great stability and antifouling properties of the nanoscaffolds, as previously demonstrated by spectroscopic ellipsometry and SPR,[33] and the well portability of the field-effect measurement station make the technology highly convenient for the rapid electronic detection of protein biomarkers.

Next, in order to compare the VS-PEI strategy with the widely employed monopyrene PBSE approach, we also modified GFETs with ConA employing this latter strategy (Figure S4A, Supporting Information). The performance of the biosensing devices toward GOx recognition was evaluated. From Figure S4B, Supporting Information, a decrease in I_{DS} is obtained upon GOx addition to the electrolyte solution, similar to what was observed for the VS-PEI approach. Furthermore, the devices also show a higher response while performing the measurements in the low ionic strength buffer solution (Figure S4C, Supporting Information). In this case, compared to the measurements performed in the high ionic strength solution, the amplitude of the biosensor response is increased by 173 ± 23% when measuring in the low ionic strength solution, displaying the same effect ascribed to the increase in the Debye length previously stated. Furthermore, K_D values of 97 ± 25 nM (R^2 = 0.95) and 46 ± 11 nM (R^2 = 0.95) for measurements in high and low ionic strength were obtained, respectively. Figure S4D, Supporting Information, shows the relative changes in I_{DS} with respect to the recognized GOx mass obtained from SPR measurements employing the same interfacial architecture on graphene-modified SPR sensors (see Experimental Section). Similar to what it was shown for VS-PEI-GFETs, a linear dependence of the biosensor response with the GOx surface coverage can be observed. A more exhaustive discussion about the implications of the experiments is found in Section 2.5.

2.3. Detection of SARS-CoV-2 Spike Protein

The COVID-19 pandemic has emphasized the necessity for rapid and sensitive SARS-CoV-2 antigen detection through robust, portable, and easy-to-handle devices for field diagnostics. SARS-CoV-2 encodes four structural proteins: spike, envelope, matrix, and nucleocapsid.[59] Among them, the spike protein is an attractive target for use as an ultrarapid diagnostic antigen because it is a major transmembrane protein of the virus and is highly immunogenic. Moreover, the spike protein enables the specific detection of SARS-CoV-2, among other coronaviruses, in nasopharyngeal swab or saliva samples.[10,60] Therefore, a mAb specific to SARS-CoV-2 S1 spike was chosen to be immobilized on GFETs for antigen detection.

The immobilization of the mAb was performed by the VS-PEI approach as described in the Experimental Section and illustrated in **Figure 4**A. GFET measurements for S1 spike detection were performed in low ionic strength PBS ×0.1 solutions due to the improved sensibility of the devices in this condition, as previously shown. From Figure 4B, the binding of the S1 spike protein to the Ab increases the I_{DS} for both functionalized devices, coherent with positively charged species adsorption, that is, a p-doping effect. Such result is consistent with the positive net charge of S1 protein at pH 7.4, as its isoelectric point is 7.80.[61] This effect has been very recently reported and employed for the construction of phononic graphene sensor,[62] and our signal behavior is in accordance with SARS-CoV-2 S1 protein biosensors based on GFETs prepared using CVD graphene.[10]

Moreover, the devices show a dynamic sensing range of 0.1–100 nM, a LOD of 0.74 nM, and a K_D^{GFET} value of 6.7 ± 0.8 nM

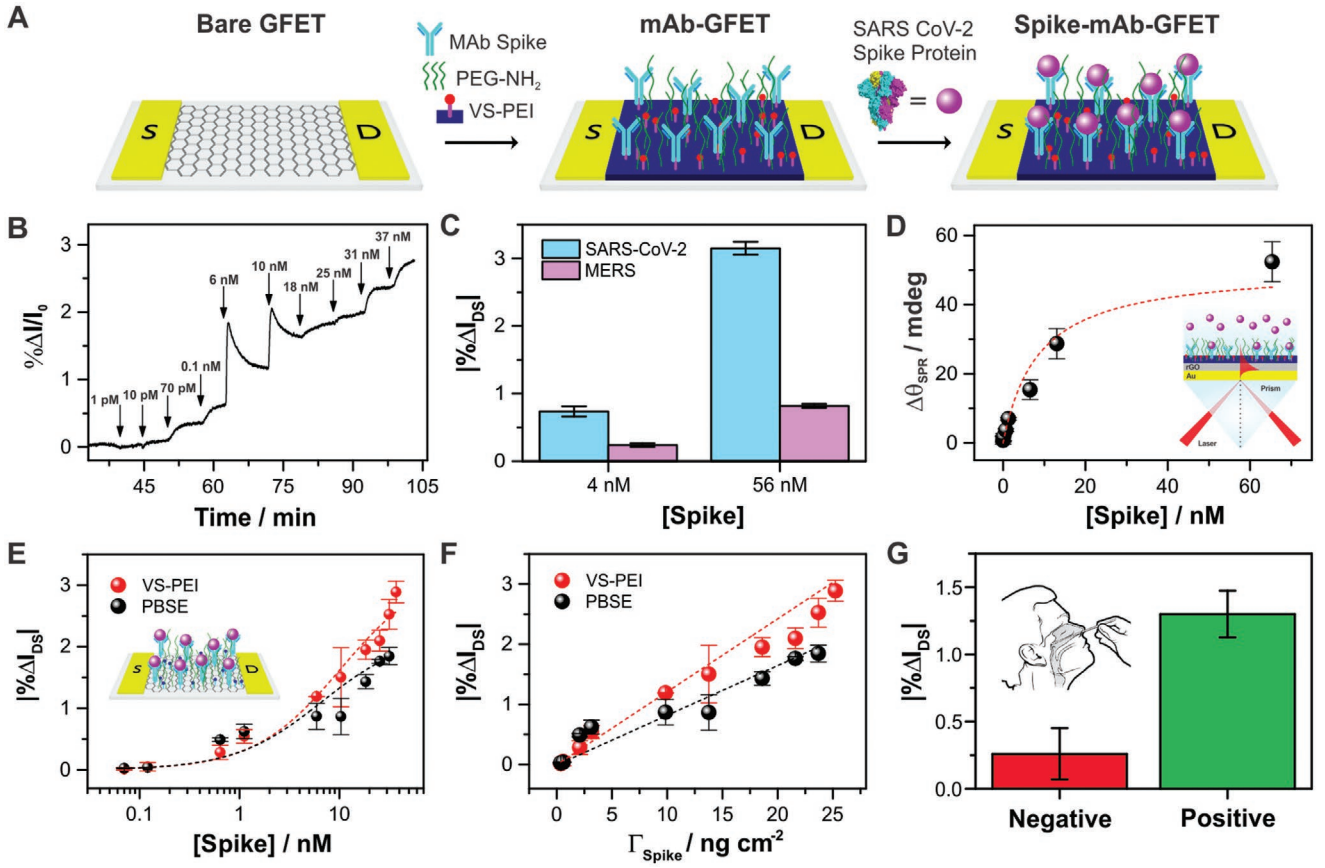

Figure 4. A) Scheme of the VS-PEI approach employed for the fabrication of the SARS-CoV-2 S1 protein biosensors. B) I_{DS} relative change for a VS-PEI-MAb-GFET upon the addition of increasing spike protein concentrations (V_{DS} = 50 mV, V_{GS} = −250 mV, PBS ×0.1 at pH 7.4). C) Results obtained from the selectivity assay employing the spike MERS protein compared with SARS-CoV2. D) Change in the SPR angle upon flowing spike solution through the SPR cell for a VS-PEI-modified SPR sensor and scheme of the SPR measurement setup. E) I_{DS} relative change comparing both approaches (n = 2). F) Relative changes in I_{DS} as a function of the SARS-CoV-2 spike protein surface mass density obtained from SPR measurements for both strategies. G) SARS-CoV-2 S1 detection results in spiked nasopharyngeal swab samples (error corresponds to three independent measurements).

(results are shown in Figure 4E for the sake of clarity). The LOD of the biosensors is adequate to detect SARS-CoV-2 spike in saliva or nasopharyngeal swab samples.[38] It should be noted that, since the ΔI_{DS} obtained at the LOD is 0.28 µA and I_{DS}^{rms} of the devices is 0.068 µA, the GFET technology is highly reliable even at the LOD. Moreover, the specificity of the biosensors was evaluated against the detection of MERS-CoV spike protein. Figure 4C shows that the biosensors have a specific response to SARS-CoV-2 spike protein (in terms of the positivity criterion obtained from Figure 4G), thus supporting the use of this approach to fabricate COVID-19 diagnostic devices.

The specific binding between the S1 spike and mAb was also studied by SPR (Figure 4D) and a K_D^{SPR} of 8.5 nM (±1.8 nM, R^2 = 0.93) was estimated. To correlate GFET and SPR results, the relative changes in I_{DS} with respect to the estimated S1 spike surface mass density (Γ_{spike}) are also presented in Figure 4F. It can be observed that the dependence of the biosensor response with the S1 Γ_{spike} is linear up to ≈30 ng cm^{-2} with a slope of 0.12%ΔI_{DS}/ng cm^{-2}. Next, the immobilization of the mAb specific against SARS-CoV-2 spike protein was also performed by the PBSE approach (as illustrated in the scheme of Figure S5, Supporting Information) using a similar protocol as previously reported.[10] GFET measurements of increasing concentrations of SARS-CoV-2 S1 spike were carried out (Figure S5, Supporting Information, and Figure 4E), and a LOD of 0.72 nM and a K_D^{GFET} of 10.4 ± 1.3 nM were obtained. It is observed that the devices fabricated with the VS-PEI approach show a better performance than those obtained by the widely employed PBSE strategy. A detailed discussion of the comparison between both approaches is found in Section 2.5.

To investigate the practical applicability of the GFET biosensing technology, SARS-CoV-2 spike protein detection was studied in spiked nasopharyngeal swab samples. The nasopharyngeal swab samples were collected from a healthy volunteer who was negative to the SARS-CoV-2 test by RT-PCR. Then, the samples were spiked with SARS-CoV-2 S1 protein (i.e., positive samples) and subjected to electronic measurement (see Section 4.3 for sample preparation details). As shown in Figure 4G, the biosensor response to the positive samples was considerably higher than the obtained to the negative samples. For the analysis of spiked nasopharyngeal swab samples, a SARS-CoV-2 S1 assay result was considered positive if it was equal or higher than a cutoff threshold of 3 × standard deviation (SD) of the negative control samples above the assay

background, in accordance with ICH Quality Guidelines and other bioelectronics antigen assays.[63,64] Based on this criterion, the electronic test showed sensitivity and selectivity both of 100%.

To understand whether the sensing features of the biosensors are adequate for S1 detection in clinical samples with SARS-CoV-2 variants of concern, S1 concentration was estimated from the viral load reported in nasopharyngeal samples. Puhach et al. reported $10^{7.5}$–≈$10^{9.5}$ viral RNA copies/mL for Omicron and Delta variants,[65] while Earnest et al. reported an average of 10^7.3 viral RNA copies/mL for Delta variant.[66] Thus, a range from $10^{7.3}$ to $10^{9.5}$ viral RNA copies/mL can be considered. In addition, there are ≈50 spike trimmers per virus particle,[67] and each spike monomer has one S1 subunit; so, there are ≈150 S1 proteins per virion. Therefore, a range from 0.05 to 7.8 nM S1 is estimated for nasopharyngeal samples (see Supporting Information for calculation details). Thus, our GFET biosensors with a LOD of 0.74 nM could detect positively a large fraction of the clinical samples from COVID-19 patients.

In addition, since VS-PEI nanoscaffolds can easily bind different mAbs, as demonstrated in this and previous works,[33] the advent of new commercially available mAbs with higher affinity could lead to the development of GFETs with even higher sensitivity, able to detect most of the positive clinical samples.

2.4. Detection of Ferritin

Finally, we studied the detection of human ferritin by GFETs modified with mAbs specific against the ferritin heavy chain (FTH1). Serum ferritin level increase is associated to a higher probability of developing or continuing a cytokine storm in COVID-19 patients.[68] Therefore, ferritin is considered a good indicator of the COVID-19 inflammatory response, and its value can be used to perform an assessment of clinical progress and provides alertness on critical patients.[1,69] FTH1-mAb and PEG were anchored on GFETs by the VS-PEI scaffold (left panel of **Figure 5**A), as described in the Experimental Section. The measurements were performed at HEPES buffer ×0.1 pH 7.4. From Figure 5B, the recognition of the ferritin to the platforms yields a decrease in I_{DS}, that is, an n-doping effect, consistently with its negative net charge (the isoelectric point is 5.5).[70] Furthermore, the biosensors show a I_{DS} dynamic range of 0.1–10 nM, a LOD of 0.23 nM, and a K_D^{GFET} value of 8.8 ± 1.5 nM (Figure 5C). Since it has been reported that COVID-19 patients with poor clinical progress present hyperferritinemia, that is, ferritin serum levels higher than 500 μg L^{-1} (1.04 nM),[71,72] the GFET technology becomes promising to assess the presence of hyperinflammation and to predict the aggravation in COVID-19 patients.[73] In this system, the specificity was evaluated by monitoring the electric response for BSA-modified GFETs during the addition of ferritin. Figure 5G shows that only the biosensors fabricated with the Ab display a response to ferritin, supporting the use of this approach to fabricate ferritin sensing devices.

Figure 5D shows the relative changes in I_{DS} with respect to the $\Gamma_{Ferritin}$ obtained from previously reported SPR measurements employing the same interfacial architecture.[33] A good linear correlation up to ≈45 ng cm^{-2} with a slope of 0.073% ΔI_{DS}/ng cm^{-2} and a good agreement between K_D values (8.8 and 15.0 nM by GFET and SPR, respectively) can be observed. Furthermore, the immobilization of the FTH1-mAb was also done by the PBSE approach (as illustrated in the right scheme of Figure 5A). GFET measurements of increasing concentrations of ferritin were carried out with these sensors yielding a LOD of 0.53 nM and a K_D^{GFET} of 11.8 ± 3.2 nM (Figure S6, Supporting Information, and Figure 5C).

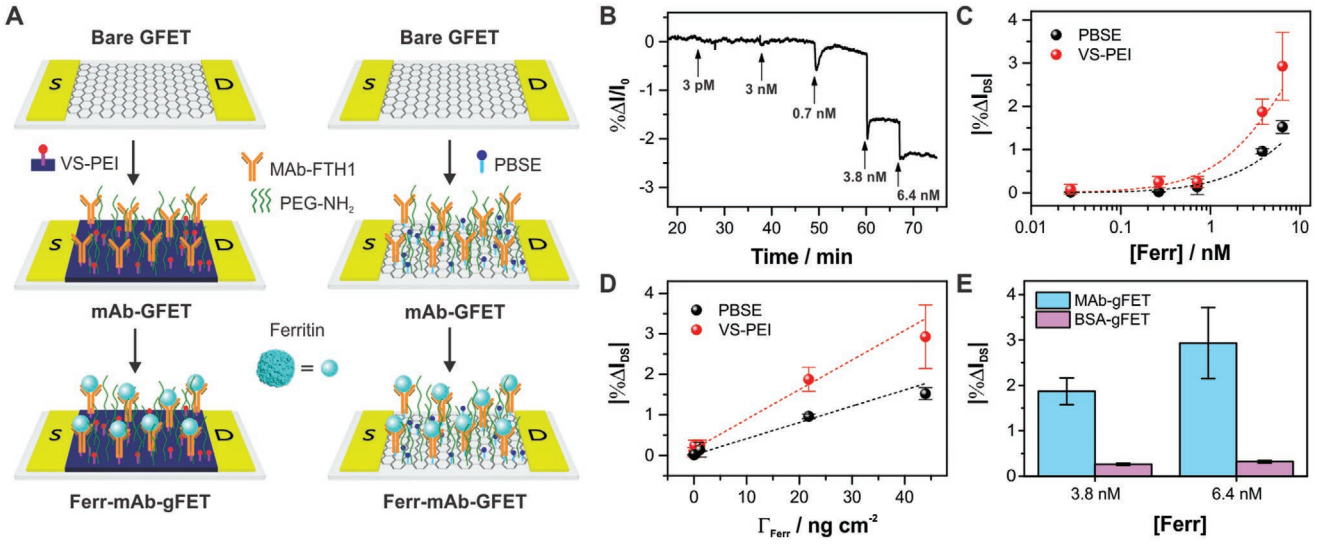

Figure 5. A) Scheme of the fabrication of ferritin biosensors, by VS-PEI (left) and PBSE (right) approaches. B) Relative change in I_{DS} for a MAb-VS-PEI-GFET upon the addition of different ferritin concentrations (V_{DS} = 50 mV, V_{GS} = –250 mV, HEPES buffer ×0.1 at pH 7.4). C) Results obtained for the two different approaches (n = 2). D) Relative changes in I_{DS} for deposited ferritin surface mass density obtained from SPR measurements for both strategies. E) Specificity experiment for ferritin sensing by BSA and mAb-modified GFETs.

2.5. GFETs—SPR Correlation and Comparison between Bio-Immobilization Approaches

In general, it is considered that the recognition of charged target molecules leads to a GFET response caused by changes in the Donnan potential and the electrostatic potential at the graphene interface.[18] Moreover, some models that describe the GFET sensing response were previously reported.[40,57,74] Nevertheless, for a rigorous validation of the GFET-based biosensing technology, it is still necessary to correlate the GFET response with the recognized surface mass obtained by a reference method. To achieve this goal, SPR measurements were performed, since it is the gold standard technique to study affinity systems on surfaces.[75–77] Thus, the same interfacial architectures were constructed on graphene-SPR sensors and the surface concentrations (Γ) of the different biomolecules were calculated from the changes in the angular dependence of the sensor's reflectivity. Then, the SPR results were compared with those obtained with GFET sensors. As depicted in Figure S4D,H, Supporting Information, and Figure 5D, for all the studied protein–protein recognition systems and for both immobilization approaches (i.e., VS-PEI and PBSE), GFET responses correlate linearly with targets surface concentration (Γ) up to 100 ng cm^{-2}, showing adequate "goodness of fits" ($R^2 > 0.90$). The directly proportional relation between Γ and $\%I_{DS}$ suggests that the biosensing platform response follows a Debye–Huckel model-like behavior;[78] that is, (for low interface potentials) the potential at the graphene surface (ψ) can be expressed as $\psi = \sigma\lambda_D/\varepsilon\varepsilon_0$, where σ is the charge density and λ_D the Debye length. This deduction can be understood as follows, since the σ of the recognized proteins is proportional to Γ, and $\Delta\%I_{DS}$ is proportional to $\Delta\psi$ ($\Delta\% I_{DS} = g_m\Delta\psi$), therefore $\Delta\%I_{DS} \propto \Gamma$.

From the same correlations and using the LOD obtained values, it is derived that the transistors could sense surface mass changes as low as 2 ng cm^{-2}. Furthermore, K_D values obtained by GFET sensors are in excellent agreement with those obtained by SPR (**Figure 6**A). These results show the high reliability of the GFET technology for sensing target biomolecules and also for the investigation of molecule–molecule affinity constants, yielding values similar to those obtained by SPR while requiring simpler equipment, less amount of reagents, and less operative time.

Since the studied target molecules and recognition elements have different isoelectric points, molecular weights, and net charges, it is expected that GFET technology display different sensitivity for each system. To analyze this point in deep, slope values obtained from the linear regressions of I_{DS} as a function of Γ are shown in Figure 6B. It can be seen that higher slope values are obtained for the mAb-antigen systems in comparison to the lectin-glycoprotein one. This suggests that the recognition element properties such as its charge, size, and molecular structure impact directly on the sensitivity of the sensors, in agreement with previous reports.[18,79,80]

It is also interesting to compare the GFET sensing features resulting from both immobilization approaches used in this work. From Figures 2C, 4G, and 5C and Figure S4C, Supporting Information, it is observed that the GFET-based biosensors employing the VS-PEI approach show better sensitivities, higher sensing amplitudes (see Figure S7, Supporting Information), and similar LODs. In addition, from the linear regressions of I_{DS} as a function of Γ (Figure 6B), higher slope values are displayed for VS-PEI-functionalized GFETs in all the systems. It is worth noting that the VS-PEI approach leads to a higher distance between the graphene and the recognition element than PBSE which, at a first glance, seems to result in a decrease of the GFET sensitivity due to ionic screening. Nevertheless, polymer interfaces can improve the transistors sensing features.[19] In particular, as previously demonstrated both experimentally and theoretically, polyelectrolyte films are capable to extend the sensing range of GFETs by increasing the Debye length by more than one order of magnitude.[57] This enhancement results mainly from the entropic cost of confining ions inside the polymer film. For instance, when considering measurements in physiological conditions, it has been proved that polyelectrolyte films can increase the sensing range from 0.82 to 9.6 nm, which has major consequences for the construction of biosensors. This phenomenon may yield the enhanced response of the biosensors constructed by the nanoscaffold strategy.

3. Conclusions

We have developed a novel approach for functionalizing GFETs to be used as biosensors. This approach involves the construction of a VS-PEI interfacial architecture containing reactive groups for the covalent immobilization of recognition elements together with antifouling elements. Different types of binding-protein were immobilized on the graphene surface to study different protein–protein recognition equilibria. First, a lectin (ConA) was immobilized on the VS-PEI nanoscaffold, and the

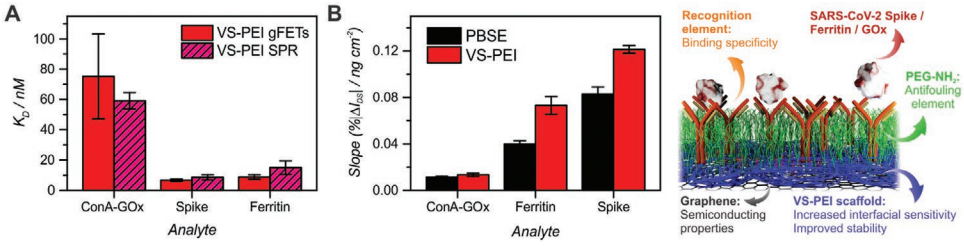

Figure 6. A) Comparison of obtained K_D values from fittings of the SPR data and the data obtained with FETs. B) Comparison of the slopes obtained with both approaches for the different systems evaluated; and a scheme of the main features presented in the biosensors that use VS-PEI nanoscaffolds. The error bars correspond to the values obtained from the fitting.

binding of GOx was detected by the changes in the I_{DS} induced by the glycoprotein-lectin biorecognition interaction. Moreover, the spike protein of the SARS-CoV-2 virus was also detected by GFETs biosensors previously functionalized with specific Abs, and their specificity was evaluated against the spike protein of the MERS virus. SARS-CoV-2 spike protein biosensors were further evaluated in spiked nasopharyngeal swab samples, displaying sensitivity and selectivity both of 100%. In other words, all the nasopharyngeal swab samples (from a healthy volunteer) spiked with S1 SARS-CoV-2 antigen were detected as "positive test results" by the sensors, while no false-positive test results were obtained from control samples without SARS-CoV-2 S1 antigen. Furthermore, ferritin biosensors were also fabricated by this approach using mAbs-functionalized GFETs which detected human ferritin with a very low LOD. On the other hand, the VS-PEI strategy was validated by functionalizing graphene-modified SPR sensors with the same interfacial architecture, and the amount of analyte adsorbed was correlated to the response of the GFETs-based biosensors. Finally, the approach developed was compared to the widely employed PBSE-based approach, showing better performance in terms of signal amplitude, sensitivity, and detection limits. This work introduces an appealing strategy for the development of novel GFET-based biosensing devices, overcoming common problems of the pyrene-based approach such as low stability, and paves the way for reliable biosensing devices toward point-of-care and mobile health medicine.

4. Experimental Section

Materials: Dimethylformamide (DMF), Na_2CO_3, and HEPES were purchased from Anedra. DVS, 1-pyrenebutanoic acid succinimidyl ester (PBSE), PEI (750 kDa), PEG-NH_2 (10 kDa), ConA (catalog number: C2010), and human ferritin (CAS: 9007-73-2, catalog number: 341482, purity > 95% by SDS-PAGE) were purchased from Sigma-Aldrich, sodium borate from Parafarm, NaCl and KCl from Biopack, and ETA from Mallinckrodt. SARS-CoV-2 spike neutralizing mAb (source: mouse IgG1, catalog number: 400591-MM43), anti-human ferritin heavy chain 1 (FTH1) mAb (source: mouse IgG1, catalog number: 13217-MM06), SARS-CoV-2 S1 spike recombinant protein (catalog number: 40591-V08H, purity > 95% by SDS-PAGE) and MERS-CoV S1 spike protein (catalog number: 40069-V08H, purity > 95% by SDS-PAGE) were purchased from Sino Biological (USA). PBS solutions pH 7.4 were prepared from PBS tablets (Sigma-Aldrich, P4417). All solutions were prepared using milli-Q grade water. SPR sensors modified with rGO (referred to as graphene-SPR sensors) were prepared as previously described.[57,81]

Functionalization of GFET and Graphene-SPR Sensors: *VS-PEI nanoscaffolds*: Biofunctionalization and PEGylation of GFET and graphene-SPR sensors were done by vinylsulfonated-polyamine nanoscaffolds according to a previously reported procedure.[33] Briefly, the approach involved the modification of the graphene-sensors as follows (see Scheme S1, Supporting Information): 1) sensors were incubated in 5 mM PBSE in DMF for 2 h, washed with DMF and dried; 2) The sensors were then incubated in 2 mg mL^{-1} PEI at pH = 10 for 1 h, washed with deionized water and dried; 3) the VS-PEI nanoscaffolds were obtained by incubating the PBSE-polyamine-modified GFETs in 5% DVS solution in carbonate buffer (0.5 M Na_2CO_3, pH = 11) for 1 h, washed with deionized water and dried. To anchor the different recognition elements to this surface, the graphene-sensors were incubated in 100 µg mL^{-1} ConA or mAb solution in borate-buffered saline (BBS) buffer pH = 9.0 for 5 h and then washed with BBS. Next, the biosensors were incubated in 0.2 mM PEG-NH_2(10 kDa), to confer antifouling properties to the surface,[33] and subsequently incubated in 100 mM ETA, for blocking the vinylsulfone remaining groups that could have not reacted. Finally, the biosensors were washed with BBS and stored in buffer.

PBSE approach: In order to compare VS-PEI nanoscaffolds approach with a widely employed monopyrene-based approach,[10,82] the GFET and graphene-SPR sensors were first modified with PBSE and subsequently incubated in ConA or mAb solution in PBS pH = 7.4 buffer for 1.5 h (see Scheme S1, Supporting Information). Then, the substrates were incubated in 0.2 mM PEG-NH_2 (10 kDa) in PBS pH = 7.4 for 2 h and finally incubated in 100 mM ETA solution in PBS pH = 7.4 for 15 min. The biosensors were washed with PBS and stored in buffer.

GFET Measurements: Electrical measurements were performed employing a portable FET measurement station Zaphyrus-W10 (GISENS BIOTECH, Argentina). rGO field-effect transistors (GFETs) with a coplanar Ag/AgCl gate prepared by a previously reported wafer-scale method[39] were supplied by GISENS BIOTECH (further information about the fabrication and characterization of the graphene-based devices is shown in Figures S1 and S8 and Table S3, Supporting Information). The drain–source current (I_{DS}) was recorded while applying both fixed V_{DS} = 50 mV and V_{GS} = −250 mV. The cell was filled with 200 µL buffer solution and the measurements were started. Volumes of different analyte/protein concentration solutions prepared in the same buffer were added to the cell to reach the final analyte concentration. All measurements were performed in triplicate unless otherwise indicated. For ferritin measurements, 10 mM HEPES, 140 mM NaCl pH 7.4 buffer solution (HEPES buffer ×1), or the same buffer tenfold diluted with milli-Q water (HEPES buffer ×0.1) were used. Since Ca^{2+} was a necessary ion for the binding site of ConA, 0.5 mM $CaCl_2$ was added to the HEPES buffer for GOx measurements. SARS-CoV-2 spike protein measurements were performed in PBS ×1 or PBS ×0.1 pH 7.4.

The response of the biosensors was measured as

$$\%I_{DS} = 100\left(\frac{I_{DS} - I_{baseline}}{I_0}\right) \quad (1)$$

where the changes in I_{DS} were obtained by correction by baseline subtraction ($I_{DS} - I_{baseline}$) and I_0 was the initial current value of the GFET measurement, similar to what was previously reported.[45]

The response of all the systems (i.e., GOx-ConA, Ferritin and Spike protein) were fitted to a noncooperative Hill model (n = 1):

$$\%I_{DS} = \frac{\%I_{DS,max} C}{C + K_D^{GFET}} \quad (2)$$

where $\%I_{DS,max}$ was the maximum GFET response, C was the target concentration, and K_D^{GFET} was the apparent affinity constant.

The LOD of the biosensors was determined as three times the average of the standard deviation of two different blank injections. I_{DS}^{rms} were obtained from 1-min I_{DS} measurements using V_{DS} = 50 mV and V_{GS} = −250 mV in PBS ×0.1. First, mean values of I_{DS} ($<I_{DS}>$) were calculated and then, these values were extracted from the I_{DS} (i.e., $I_{DS} - <I_{DS}>$). Finally, their root mean square (rms) values were calculated.

SARS-CoV-2 S1 protein detection in spiked nasopharyngeal swab samples: The nanopharyngeal swab samples were collected from a healthy volunteer who was negative to the SARS-CoV-2 test by RT-PCR. An informed consent was obtained from the volunteer. The swab samples were extracted in 1 mL of PBS pH 7.4 for 10 min. To prepare the positive samples, 56 nM SARS-CoV-2 S1 protein was added to the nasopharyngeal sample extracts. Negative (control) samples were nasopharyngeal swab extracts in the absence of antigen. From the tests results, selectivity (TN/(TN+FP)) and sensitivity (TP/(TP+FN)) values were calculated.

SPR Measurements: A multiparametric SPR instrument SPR Navi 210 A (BioNavis, Finland) was used to monitor the binding between the recognition elements and the target molecules. SPR measurements were carried out using a flow rate of 20 µL min^{-1} and a 670 nm laser. The response at the steady states (i.e., at the equilibrium) of the SPR angle shifts ($\Delta\theta_{SPR}$) was obtained as a function of the protein concentration (C). Then, apparent equilibrium dissociation constants (K_D^{SPR}) were

determined by fitting the experimental data with a noncooperative Hill model:[83,84]

$$\Delta\theta_{SPR} = \frac{\Delta\theta_{SPR,max} C}{C + K_D^{SPR}} \quad (3)$$

where $\Delta\theta_{SPR,\,max}$ was the maximum binding capacity. Each system was measured and analyzed in duplicate. Surface mass density estimation was performed as described elsewhere[25] and using a $d\eta/dC$ value of 1.77×10^{-10} cm^3 ng^{-1}. All measurements were performed in duplicate.

Supporting Information

Supporting Information is available from the Wiley Online Library or from the author.

Acknowledgements

E.P. and G.E.F. contributed equally to this work. This work was supported by the following institutions: Universidad Nacional de La Plata (UNLP), ANPCYT (PICT 2018-04684 and EBT COVID-19 No. 0017-IF-2020-85480721-APN-FONARSEC#ANPIDTYI), GISENS BIOTECH, and CONICET-UNLP-GISENS BIOTECH (700-2845/20-000). J.S., W.A.M., and O.A. are staff members of CONICET. J.A.A., G.E.F., and E.P. acknowledge their fellowship from CONICET.

Conflict of Interest

E.P., W.A.M., and O.A. are scientific advisors of GISENS BIOTECH through a contract between UNLP, CONICET, and GISENS BIOTECH. A.L.C. and J.M.P. are recently or presently employed by GISENS BIOTECH. The other authors declare no conflict of interest.

Data Availability Statement

The data that support the findings of this study are available from Gisens Biotech. Restrictions apply to the availability of these data, which were used under license for this study. Data are available from the authors with the permission of Gisens Biotech.

Keywords

COVID-19, ferritin, field-effect transistors, graphene, severe acute respiratory-related coronavirus 2, spike protein, surface plasmon resonance

Received: December 22, 2021
Revised: February 4, 2022
Published online:

[1] E. Morales-Narváez, C. Dincer, *Biosens. Bioelectron.* **2020**, *163*, 112274.
[2] A. Endo, S. Abbott, A. J. Kucharski, S. Funk, *Wellcome Open Res.* **2020**, *5*, 67.
[3] D. C. Adam, P. Wu, J. Y. Wong, E. H. Y. Lau, T. K. Tsang, S. Cauchemez, G. M. Leung, B. J. Cowling, *Nat. Med.* **2020**, *26*, 1714.
[4] *SARS-CoV-2 Antigen-Detecting Rapid Diagnostic Tests: An Implementation Guide*, World Health Organization, Geneva, **2020**.
[5] D. Shan, J. M. Johnson, S. C. Fernandes, H. Suib, S. Hwang, D. Wuelfing, M. Mendes, M. Holdridge, E. M. Burke, K. Beauregard, Y. Zhang, M. Cleary, S. Xu, X. Yao, P. P. Patel, T. Plavina, D. H. Wilson, L. Chang, K. M. Kaiser, J. Nattermann, S. V. Schmidt, E. Latz, K. Hrusovsky, D. Mattoon, A. J. Ball, *Nat. Commun.* **2021**, *12*, 1931.
[6] R. Wölfel, V. M. Corman, W. Guggemos, M. Seilmaier, S. Zange, M. A. Müller, D. Niemeyer, T. C. Jones, P. Vollmar, C. Rothe, M. Hoelscher, T. Bleicker, S. Brünink, J. Schneider, R. Ehmann, K. Zwirglmaier, C. Drosten, C. Wendtner, *Nature* **2020**, *581*, 465.
[7] N. R. Pollock, T. J. Savage, H. Wardell, R. A. Lee, A. Mathew, M. Stengelin, G. B. Sigal, *J. Clin. Microbiol.* **2021**, *59*, 1.
[8] G. C. Mak, S. S. Lau, K. K. Wong, N. L. Chow, C. Lau, E. T. Lam, R. C. Chan, D. N. Tsang, *J. Clin. Virol.* **2020**, *133*, 104684.
[9] A. Scohy, A. Anantharajah, M. Bodéus, B. Kabamba-Mukadi, A. Verroken, H. Rodriguez-Villalobos, *J. Clin. Virol.* **2020**, *129*, 104455.
[10] G. Seo, G. Lee, M. J. Kim, S.-H. Baek, M. Choi, K. B. Ku, C.-S. Lee, S. Jun, D. Park, H. G. Kim, S.-J. Kim, J.-O. Lee, B. T. Kim, E. C. Park, S. I. Kim, *ACS Nano* **2020**, *14*, 5135.
[11] A. Zhang, C. M. Lieber, *Chem. Rev.* **2016**, *116*, 215.
[12] G. E. Fenoy, C. Bilderling, W. Knoll, O. Azzaroni, W. A. Marmisollé, *Adv. Electron. Mater.* **2021**, *7*, 2100059.
[13] D. C. Christodouleas, B. Kaur, P. Chorti, *ACS Cent. Sci.* **2018**, *4*, 1600.
[14] K. J. Land, D. I. Boeras, X.-S. Chen, A. R. Ramsay, R. W. Peeling, *Nat. Microbiol.* **2019**, *4*, 46.
[15] S. Su, Q. Sun, X. Gu, Y. Xu, J. Shen, D. Zhu, J. Chao, C. Fan, L. Wang, *TrAC, Trends Anal. Chem.* **2019**, *119*, 115610.
[16] G. E. Fenoy, W. A. Marmisollé, O. Azzaroni, W. Knoll, *Biosens. Bioelectron.* **2020**, *148*, 111796.
[17] K. S. Novoselov, A. K. Geim, S. V. Morozov, D. Jiang, Y. Zhang, S. V. Dubonos, I. V. Grigorieva, A. A. Firsov, *Science* **2004**, *306*, 666.
[18] W. Fu, L. Jiang, E. P. Van Geest, L. M. C. Lima, G. F. Schneider, *Adv. Mater.* **2017**, *29*, 1603610.
[19] N. Gao, T. Gao, X. Yang, X. Dai, W. Zhou, A. Zhang, C. M. Lieber, *Proc. Natl. Acad. Sci. USA* **2016**, *113*, 14633.
[20] T. Reiss, K. Hjelt, A. C. Ferrari, *Nat. Nanotechnol.* **2019**, *14*, 907.
[21] B. Deng, Z. Liu, H. Peng, *Adv. Mater.* **2019**, *31*, 1800996.
[22] Y. Li, N. Chopra, *JOM* **2015**, *67*, 34.
[23] X. Zhang, Q. Jing, S. Ao, G. F. Schneider, D. Kireev, Z. Zhang, W. Fu, *Small* **2020**, *16*, 1902820.
[24] E. Piccinini, C. Bliem, C. Reiner-Rozman, F. Battaglini, O. Azzaroni, W. Knoll, *Biosens. Bioelectron.* **2017**, *92*, 661.
[25] T. Berninger, C. Bliem, E. Piccinini, O. Azzaroni, W. Knoll, *Biosens. Bioelectron.* **2018**, *115*, 104.
[26] S. Niyogi, E. Bekyarova, M. E. Itkis, H. Zhang, K. Shepperd, J. Hicks, M. Sprinkle, C. Berger, C. N. Lau, W. A. Deheer, E. H. Conrad, R. C. Haddon, *Nano Lett.* **2010**, *10*, 4061.
[27] A. Ramasubramaniam, R. Selhorst, H. Alon, M. D. Barnes, T. Emrick, D. Naveh, *J. Mater. Chem. C* **2017**, *5*, 11158.
[28] K. R. Nandanapalli, D. Mudusu, S. Lee, *Carbon* **2019**, *152*, 954.
[29] M. Kohmoto, H. Ozawa, Li Yang, T. Hagio, M. Matsunaga, M.-A. Haga, *Langmuir* **2016**, *32*, 4141.
[30] M. Cao, A. Fu, Z. Wang, J. Liu, N. Kong, X. Zong, H. Liu, J. J. Gooding, *J. Phys. Chem. C* **2014**, *118*, 2650.
[31] J. A. Mann, T. Alava, H. G. Craighead, W. R. Dichtel, *Angew. Chem., Int. Ed.* **2013**, *52*, 3177.
[32] J. A. Mann, J. Rodríguez-López, H. D. Abruña, W. R. Dichtel, *J. Am. Chem. Soc.* **2011**, *133*, 17614.
[33] E. Piccinini, J. A. Allegretto, J. Scotto, A. L. Cantillo, G. E. Fenoy, W. A. Marmisollé, O. Azzaroni, *ACS Appl. Mater. Interfaces* **2021**, *13*, 43696.
[34] X. Li, S. Yu, T. Yan, Y. Zhang, B. Du, D. Wu, Q. Wei, *Biosens. Bioelectron.* **2017**, *89*, 1020.
[35] C. M. Miyazaki, R. Mishra, D. J. Kinahan, M. Ferreira, J. Ducrée, *Colloids Surf., B* **2017**, *158*, 167.

[36] E. K. G. Trindade, B. V. M. Silva, R. F. Dutra, *Biosens. Bioelectron.* **2019**, *138*, 111311.
[37] X. Zhao, J. Wang, H. Chen, H. Xu, L. Bai, W. Wang, H. Yang, D. Wei, B. Yuan, *Sens. Actuators, B* **2019**, *301*, 127071.
[38] H.-Y. Kim, J.-H. Lee, M. J. Kim, S. C. Park, M. Choi, W. Lee, K. B. Ku, B. T. Kim, E. C. Park, H. G. Kim, S. I. Kim, *Biosens. Bioelectron.* **2021**, *175*, 112868.
[39] J. M. Piccinini, O. Azzaroni, E. Piccinini, W. A. Marmisolle, J. A. Allegretto, J. Scotto, A. L. Cantillo, G. E. Fenoy, *WO 2021240440A1*, **2021**.
[40] B. R. Goldsmith, L. Locascio, Y. Gao, M. Lerner, A. Walker, J. Lerner, J. Kyaw, A. Shue, S. Afsahi, D. Pan, J. Nokes, F. Barron, *Sci. Rep.* **2019**, *9*, 434.
[41] N. Gao, W. Zhou, X. Jiang, G. Hong, T.-M. Fu, C. M. Lieber, *Nano Lett.* **2015**, *15*, 2143.
[42] D. Khodagholy, J. Rivnay, M. Sessolo, M. Gurfinkel, P. Leleux, L. H. Jimison, E. Stavrinidou, T. Herve, S. Sanaur, R. M. Owens, G. G. Malliaras, *Nat. Commun.* **2013**, *4*, 2133.
[43] M. Berto, S. Casalini, M. Di Lauro, S. L. Marasso, M. Cocuzza, D. Perrone, M. Pinti, A. Cossarizza, C. F. Pirri, D. T. Simon, M. Berggren, F. Zerbetto, C. A. Bortolotti, F. Biscarini, *Anal. Chem.* **2016**, *88*, 12330.
[44] R. Garcia-Cortadella, G. Schwesig, C. Jeschke, X. Illa, A. L. Gray, S. Savage, E. Stamatidou, I. Schiessl, E. Masvidal-Codina, K. Kostarelos, A. Guimerà-Brunet, A. Sirota, J. A. Garrido, *Nat. Commun.* **2021**, *12*, 1.
[45] R. Hajian, S. Balderston, T. Tran, T. Deboer, J. Etienne, M. Sandhu, N. A. Wauford, J.-Y. Chung, J. Nokes, M. Athaiya, J. Paredes, R. Peytavi, B. Goldsmith, N. Murthy, I. M. Conboy, K. Aran, *Nat. Biomed. Eng.* **2019**, *3*, 427.
[46] N. M. Andoy, M. S. Filipiak, D. Vetter, Ó. Gutiérrez-Sanz, A. Tarasov, *Adv. Mater. Technol.* **2018**, *3*, 1800186.
[47] N. Schaefer, R. Garcia-Cortadella, A. B. Calia, N. Mavredakis, X. Illa, E. Masvidal-Codina, J. De La Cruz, E. D. Corro, L. Rodríguez, E. Prats-Alfonso, J. Bousquet, J. Martínez-Aguilar, A. P. Pérez-Marín, C. Hébert, R. Villa, D. Jiménez, A. Guimerà-Brunet, J. A. Garrido, *Carbon* **2020**, *161*, 647.
[48] L. D. Sappia, E. Piccinini, C. Von Binderling, W. Knoll, W. Marmisollé, O. Azzaroni, *Mater. Sci. Eng., C* **2020**, *109*, 110575.
[49] F. Cheng, J. Shang, D. M. Ratner, *Bioconjugate Chem.* **2011**, *22*, 50.
[50] J. Shang, F. Cheng, M. Dubey, J. M. Kaplan, M. Rawal, X. Jiang, D. S. Newburg, P. A. Sullivan, R. B. Andrade, D. M. Ratner, *Langmuir* **2012**, *28*, 3338.
[51] B. Fei, Z. Yang, S. Shao, S. Wan, J. H. Xin, *Polymer* **2010**, *51*, 1845.
[52] Y. Y. Wang, P. J. Burke, *Nano Res.* **2014**, *7*, 1650.
[53] F. P. Schwarz, K. D. Puri, R. G. Bhat, A. Surolia, *J. Biol. Chem.* **1993**, *268*, 7668.
[54] J.-I. Anzai, Y. Kobayashi, T. Hoshi, H. Saiki, *Chem. Lett.* **1999**, *28*, 365.
[55] J.-I. Anzai, Y. Kobayashi, N. Nakamura, T. Hoshi, *Sens. Actuators, B* **2000**, *65*, 94.
[56] R. Wilson, A. P. F. Turner, *Biosens. Bioelectron.* **1992**, *7*, 165.
[57] E. Piccinini, S. Alberti, G. S. Longo, T. Berninger, J. Breu, J. Dostalek, O. Azzaroni, W. Knoll, *J. Phys. Chem. C* **2018**, *122*, 10181.
[58] D. Mislovičová, J. Katrlík, E. Paulovičová, P. Gemeiner, J. Tkac, *Colloids Surf., B* **2012**, *94*, 163.
[59] Y. M. Bar-On, A. Flamholz, R. Phillips, R. Milo, *eLife* **2020**, *9*, 1.
[60] A. Yakoh, U. Pimpitak, S. Rengpipat, N. Hirankarn, O. Chailapakul, S. Chaiyo, *Biosens. Bioelectron.* **2021**, *176*, 112912.
[61] F. Krebs, C. Scheller, K. Grove-Heike, L. Pohl, H. Wätzig, *Electrophoresis* **2021**, *42*, 687.
[62] N. H. L. Nguyen, S. Kim, G. Lindemann, V. Berry, *ACS Nano* **2021**, *15*, 11743.
[63] K. Guo, S. Wustoni, A. Koklu, E. Díaz-Galicia, M. Moser, A. Hama, A. A. Alqahtani, A. N. Ahmad, F. S. Alhamlan, M. Shuaib, A. Pain, I. Mcculloch, S. T. Arold, R. Grünberg, S. Inal, *Nat. Biomed. Eng.* **2021**, *5*, 666.
[64] L. Fabiani, M. Saroglia, G. Galatà, R. De Santis, S. Fillo, V. Luca, G. Faggioni, N. D'amore, E. Regalbuto, P. Salvatori, G. Terova, D. Moscone, F. Lista, F. Arduini, *Biosens. Bioelectron.* **2021**, *171*, 112686.
[65] O. Puhach, K. Adea, N. Hulo, P. Sattonnet, C. Genecand, A. Iten, F. J. Bausch, L. Kaiser, P. Vetter, I. Eckerle, B. Meyer, *medRxiv* **2022**, DOI: https://doi.org/10.1101/2022.01.10.22269010.
[66] R. Earnest, R. Uddin, N. Matluk, N. Renzette, K. J. Siddle, C. Loreth, G. Adams, C. H. Tomkins-Tinch, M. E. Petrone, J. E. Rothman, M. I. Breban, R. T. Koch, K. Billig, J. R. Fauver, C. B. F. Vogels, S. Turbett, K. Bilguvar, B. De Kumar, M. L. Landry, D. R. Peaper, K. Kelly, G. Omerza, H. Grieser, S. Meak, J. Martha, H. H. Dewey, S. Kales, D. Berenzy, K. Carpenter-Azevedo, E. King, *medRxiv* **2021**, DOI: https://doi.org/10.1101/2021.10.06.21264641.
[67] S. Klein, M. Cortese, S. L. Winter, M. Wachsmuth-Melm, C. J. Neufeldt, B. Cerikan, M. L. Stanifer, S. Boulant, R. Bartenschlager, P. Chlanda, *Nat. Commun.* **2020**, *11*, 5885.
[68] J. Wang, M. Jiang, X. Chen, L. J. Montaner, *J. Leukocyte Biol.* **2020**, *108*, 17.
[69] F. Zhou, T. Yu, R. Du, G. Fan, Y. Liu, Z. Liu, J. Xiang, Y. Wang, B. Song, X. Gu, L. Guan, Y. Wei, H. Li, X. Wu, J. Xu, S. Tu, Y. Zhang, H. Chen, B. Cao, *Lancet* **2020**, *395*, 1054.
[70] A. Mazur, I. Litt, E. Shorr, *J. Biol. Chem.* **1950**, *187*, 473.
[71] C. E. Allen, X. Yu, C. A. Kozinetz, K. L. Mcclain, *Pediatr. Blood Cancer* **2008**, *50*, 1227.
[72] H. Senjo, T. Higuchi, S. Okada, O. Takahashi, *Hematology* **2018**, *23*, 817.
[73] L. Cheng, H. Li, L. Li, C. Liu, S. Yan, H. Chen, Y. Li, *J. Clin. Lab. Anal.* **2020**, *34*, 1.
[74] S. O. Woo, J. Froberg, Y. Pan, S. Tani, B. R. Goldsmith, Z. Yang, Y. Choi, *ACS Appl. Electron. Mater.* **2020**, *2*, 913.
[75] E. Stenberg, B. Persson, H. Roos, C. Urbaniczky, *J. Colloid Interface Sci.* **1991**, *143*, 513.
[76] Jiří Homola, S. S. Yee, G. Gauglitz, *Sens. Actuators, B* **1999**, *54*, 3.
[77] W. Knoll, *Annu. Rev. Phys. Chem.* **1998**, *49*, 569.
[78] P. Aspermair, U. Ramach, C. Reiner-Rozman, S. Fossati, B. Lechner, S. E. Moya, O. Azzaroni, J. Dostalek, S. Szunerits, W. Knoll, J. Bintinger, *J. Am. Chem. Soc.* **2020**, *142*, 11709.
[79] E. Stern, R. Wagner, F. J. Sigworth, R. Breaker, T. M. Fahmy, M. A. Reed, *Nano Lett.* **2007**, *7*, 3405.
[80] R. Elnathan, M. Kwiat, A. Pevzner, Y. Engel, L. Burstein, A. Khatchtourints, A. Lichtenstein, R. Kantaev, F. Patolsky, *Nano Lett.* **2012**, *12*, 5245.
[81] G. E. Fenoy, W. A. Marmisollé, W. Knoll, O. Azzaroni, *Sens. Diagn.* **2022**, *1*, 139.
[82] Z. Hao, Y. Zhu, X. Wang, P. G. Rotti, C. Dimarco, S. R. Tyler, X. Zhao, J. F. Engelhardt, J. Hone, Q. Lin, *ACS Appl. Mater. Interfaces* **2017**, *9*, 27504.
[83] D. G. Myszka, M. D. Jonsen, B. J. Graves, *Anal. Biochem.* **1998**, *265*, 326.
[84] M. Adamczyk, J. A. Moore, Z. Yu, *Methods* **2000**, *20*, 319.